



# Simulating the Impact of Particle Size Distribution on the Performance of Graphite Electrodes in Lithium-Ion Batteries

Fridolin Röder,<sup>[a, b]</sup> Sören Sonntag,<sup>[a]</sup> Daniel Schröder,<sup>[c]</sup> and Ulrike Krewer\*<sup>[a, b]</sup>

In this work we present a fundamental model-based analysis of the effect of active material particle size distribution (PSD) on graphite electrodes and their performance. We focused on the determination of the impact of differently shaped and scaled PSDs on the electrode performance, which is mainly influenced by the performance of the individual particles and their interaction. A mathematical electrode model with a distributed particle size is used for analysis to identify the different local current densities and the charging behavior of the particles. The heterogeneity provokes uneven surface overpotentials and reaction rates. Their identification facilitates the investigation of the degradation of such heterogeneous systems. In addition, we present an approach that accounts for the change of a PSD because of the restructuring of the electrode morphology

during battery usage into the mathematical model and identify the general impact of particle cracking and agglomeration on the battery performance. Moreover, the importance of PSD in Li-ion batteries is shown by comparing the results obtained with a single particle model used commonly. This comparison shows that in case of narrow distributions surface-area- and volume-based mean approximations are sufficient to predict overpotentials and electrode capacity if kinetic losses are dominated either by reaction at the surface or diffusion processes, respectively. This work indicates that the PSD and its change impact the performance and degradation of Li-ion batteries considerably. We suggest that the PSD and its evolution should be of particular interest in the study of the degradation of particle-based electrodes.

## Introduction

Electrochemical models are used widely to investigate Li-ion batteries with the aim to predict their electrochemical performance. The fact that the electrodes consist of particles of various sizes is usually neglected. The different particle sizes, for example, of the active material particles, yield a highly heterogeneous system. This is usually quantified by the particle size distribution (PSD). In this work, the impact of the PSD on the performance and its degradation of graphite electrodes is analyzed with a model-based approach.

It is presumed that the particle size itself, as well as its distribution, affects the capacity and aging behavior of Li-ion batteries significantly.<sup>[1]</sup> Although it is well known that small particles possess a better performance, the impact of the actual distribution of shape and scale is often not investigated. Moreover, several manufacturing processes are reported that yield a defined PSD for the active material in Li-ion batteries.<sup>[1,2]</sup> Thus, it is of particular interest to further elucidate how the various particle sizes influence the electrochemical performance of the electrodes.

Furthermore, the degradation of Li-ion batteries is related to the PSD of the active material. In graphite anodes, solvent co-intercalation, as well as gas evolution, can lead to particle cracking.<sup>[3–5]</sup> Additionally, the volume change of particles may cause a contact loss between particles.<sup>[4]</sup> The agglomeration of particles is observed for various materials in Li-ion batteries,<sup>[6–8]</sup> which is of particular importance for materials that undergo large volume changes<sup>[7]</sup> or employ nano-sized

particles.<sup>[8]</sup> Furthermore, several battery degradation effects are linked to high charging rates. This causes high electrochemical potentials and high intercalation rates,<sup>[4]</sup> which can differ locally with particle size in a distributed heterogeneous system. As the volume-to-surface ratio varies with size, the intercalation rate of Li through the surface of a host struc-

[a] F. Röder, S. Sonntag, Prof. U. Krewer  
Institute of Energy and Process Systems Engineering  
Technische Universität Braunschweig  
Franz-Liszt-Strasse 35, 38106 Braunschweig (Germany)  
Fax: (+49) 531 391-5932  
E-mail: u.krewer@tu-braunschweig.de  
Homepage: <http://www.tu-braunschweig.de/ines>

[b] F. Röder, Prof. U. Krewer  
Battery LabFactory Braunschweig  
Technische Universität Braunschweig  
Langer Kamp 19, 38106 Braunschweig (Germany)

[c] Dr. D. Schröder  
Physikalisch-Chemisches Institut  
Justus-Liebig-Universität Gießen  
Heinrich-Buff-Ring 17, 35392 Gießen (Germany)

The ORCID identification number(s) for the author(s) of this article can be found under <http://dx.doi.org/10.1002/ente.201600232>.

© 2016 The Authors. Published by Wiley-VCH Verlag GmbH & Co. KGaA. This is an open access article under the terms of the Creative Commons Attribution Non-Commercial License, which permits use, distribution and reproduction in any medium, provided the original work is properly cited, and is not used for commercial purposes.

Part of a Special Issue on “Li-Ion Batteries”. To view the complete issue, visit: <http://dx.doi.org/10.1002/ente.v4.12>

ture is linked to the particle size. The degradation progress might differ with the particle size of the active material in such systems.<sup>[9]</sup>

There have been several publications in the last decades that show the impact of the mean particle size on battery performance.<sup>[10,11]</sup> Farkhondeh et al. present an electrochemical model with a PSD of the active material with three different particle-size groups.<sup>[12]</sup> The PSD is, thereby, determined by using SEM. They show that neglecting the distribution of particles within the electrode largely underestimates the capacity at the end of a discharge with elevated C-rates. However, single-particle model approaches are limited as they do not describe the battery performance at higher current densities accurately, so Farkhondeh et al.<sup>[13]</sup> also present a model that includes multiple particles within the commonly used pseudo-2D battery model developed by Doyle et al.,<sup>[14]</sup> which is feasible to investigate the impact of C-rates greater than 1 C. Their work demonstrates that the effect of the PSD can be modeled (as is intended in this study). Zavalis et al.<sup>[15]</sup> uses such a multiple-particle model in combination with impedance analysis to determine a possible change in the PSD during battery cycling through parameter fitting. This means that the actual evolution is not modeled explicitly. To describe the evolution of the PSD during operation mathematically, Rinaldo et al.<sup>[16]</sup> show how to apply the theory of population balances by Marchisio et al.<sup>[17]</sup> on a nanoparticle catalyst system. To the best of our knowledge, such an approach has not been used to model the change of electrode structure in Li-ion batteries.

The PSD of the active material is a well-known property in Li-ion batteries and can be adjusted during the manufacture of battery electrodes.<sup>[1,2]</sup> However, the relationship of battery performance and degradation with particle size distribution is scarcely addressed in current research. Hence, in this work we aim to use a mathematical model that combines the electrochemical features of a battery electrode and the impact of the PSD of the active material to gain a better understanding of the performance and possible degradation of battery electrodes. This is shown with an example of graphite electrodes as they are the most commonly used anodes in Li-ion batteries. In detail, we describe a graphite electrode of a Li-ion battery mathematically with distributed particle sizes of the active material, which are adjusted intentionally to a certain PSD. We investigate the general impact of the shape and size of this distribution on the electrode per-

formance. We compare the results obtained with a single-particle model to evaluate under which conditions the PSD has to be taken into account. Furthermore, we show to what extent the PSD affects the current density at the surface of the differently sized particles as the local current density is a key property for several degradation effects. Finally, we show how the typical change of the distribution, for example, caused by the cracking or agglomeration of the active particles, can affect the performance of the Li-ion battery in a scenario-based analysis as suggested by Krewer et al.<sup>[18]</sup>

## Mathematical Model

In this section, the mathematical model is introduced. Equations are based on the single-particle approach used commonly as well as its modification by consideration of multiple particles of different sizes.

Both modeling approaches contain simplifications to single out the effect of diffusion in electrodes with different PSDs. The required assumptions and the consequential validity are shown in Table 1. Furthermore, population balances are employed to analyze the effect of the PSD and its change.

### Single-particle model

An electrode model is introduced based on the single-particle model approach used widely.<sup>[19]</sup> This model includes a charge balance equation and solid diffusion equation within the particles. The diffusion equation is written as [Eq. (1)]:

$$\frac{\partial c_{\text{Li}_s}(r)}{\partial t} = \frac{1}{r^2} \nabla (D_s r^2 \nabla c_{\text{Li}_s}(r)) \quad (1)$$

with the boundary conditions  $-D_s \nabla c_{\text{Li}_s}(r=0) = 0$  and  $-D_s \nabla c_{\text{Li}_s}(r=R_s) = J^{\text{Li}}/F$ , in which  $F$  is the Faraday constant,  $J^{\text{Li}} = j^{\text{Li}}/a_s$  is the Li reaction current density,  $a_s = 3\epsilon_s/R_s$  is the specific surface area,  $\epsilon_s$  is the active material fraction, and  $R_s$  is the particle radius. The charge balance is considered at the electrochemical double layer with [Eq. (2)]:<sup>[20,21]</sup>

$$a_s C^{\text{DL}} \frac{\partial E}{\partial t} = \hat{I} - j^{\text{Li}} \quad (2)$$

in which  $C^{\text{DL}}$  is the double layer capacitance,  $E$  is the elec-

**Table 1.** Model assumptions and consequent validity.

| No. | Assumption   | Validity   |
|-----|--|--|
| 1   | electrolyte and electrical resistance is neglected                               | low C-rates  |
| 2   | electrical potential at particle is independent of position within the electrode | low C-Rates/good wetting and homogeneous active material fraction  |
| 3   | efficient solid diffusion coefficient independent of particle size               | homogeneous particle structure   |
| 4   | particles are ideal spheres  | sphere-like particles  |
| 5   | particle and material properties independent of PSD                              | manufacturing of different PSD does not impact particle properties (e.g., efficient diffusion and activity coefficients) |

trode potential, and  $\hat{I}$  is the applied current density. The intercalation reaction at the solid particle–electrolyte interface is [Eq. (3)]:



in which Li in the solid is  $\text{Li}_s$ , vacancies in the solid are  $\text{V}_s$ , electrons in the solid are  $\text{e}_s^-$ , and Li ions in the electrolyte are  $\text{Li}_e^+$ .  $J^{\text{Li}}$  is the surface current density, which is determined by [Eq. (4)]:

$$\frac{J^{\text{Li}}}{F} = C_{\text{Li}_e^+}^0 a_{\text{Li}_e^+} k_a \exp\left(\frac{\beta_a EF}{RT}\right) - C_{\text{Li}_s}^0 a_{\text{Li}_s} C_{\text{V}_s}^0 a_{\text{V}_s} k_c \exp\left(\frac{-\beta_c EF}{RT}\right) \quad (4)$$

in which the activity coefficients  $a_i$  are either assumed to be ideal  $a_i = c_i / C_i^0$  (e.g.,  $\text{Li}_s^+$ ) or determined with a semiempirical function (e.g., for  $\text{Li}_s$  and  $\text{V}_s$ ), whereas  $C_i^0$  is the standard state concentration of species  $i$ . The relationship between the anodic and cathodic reaction rate constant is [Eq. (5)]:<sup>[22]</sup>

$$\frac{k_a}{k_c} = \frac{C_{\text{Li}_e^+}^0 C_{\text{V}_s}^0}{C_{\text{Li}_s}^0} \exp\left(-\frac{\Delta G^0}{RT}\right) \quad (5)$$

with a change in Gibbs free energy  $\Delta G^0 = \mu_{\text{Li}_e^+}^0 + \mu_{\text{V}_s}^0 - \mu_{\text{Li}_s}^0$ , in which  $\mu_i^0$  is the standard chemical potential of species  $i$ .

### Multiple-particle model

To model multiple particles, the presented model is further extended to include the effect of the PSD.<sup>[12,13,15,23]</sup> We used the framework provided in Ref. [24] to derive equations for the distributed parameters. Number density, surface area density, and volume density are determined from the number fraction density. If we assume spherical particles,  $A_s(R_s) = 4\pi R_s^2$  and  $V_s(R_s) = 4/3\pi R_s^3$  define the surface area and the volume of a particle radius  $R_s$ , respectively. This is used to determine the surface area density and the volume density based on the number density [Eqs. (6) and (7)]:

$$f_{\text{vol}}(R_s) = f_{\text{num}}(R_s) V_s(R_s) \quad (6)$$

$$f_{\text{area}}(R_s) = f_{\text{num}}(R_s) A_s(R_s) \quad (7)$$

In general, the integral over these number density functions is equal to the total surface area ratio  $a_s$  and the solid phase volume fraction  $\varepsilon_s$ , respectively, so that [Eqs. (8) and (9)]:

$$\varepsilon_s = \int_0^\infty f_{\text{vol}}(R_s) dR_s \quad (8)$$

$$a_s = \int_0^\infty f_{\text{area}}(R_s) dR_s \quad (9)$$

The relationship between the number fraction density and

number density is given by the total number of particles per volume  $n_s$  [Eq. (10)]:

$$f_{\text{num}}(R_s) = n_s \cdot h_{\text{num}}(R_s) \quad (10)$$

If we combining Equation (10) with Equations (6) and (8) we obtain [Eq. (11)]:

$$\varepsilon_s = n_s \cdot \int_0^\infty h_{\text{num}}(R_s) \cdot V_s(R_s) dR_s \quad (11)$$

With  $\varepsilon_s$ ,  $n_s$  is eliminated, and the relationship between the number fraction density and number density is introduced as [Eq. (12)]:

$$f_{\text{num}}(R_s) = \frac{\varepsilon_s \cdot h_{\text{num}}(R_s)}{\int_0^\infty h_{\text{num}}(R_s) \cdot V_s(R_s) dR_s} \quad (12)$$

The surface area fraction density  $h_{\text{area}}(R_s)$  and the volume fraction density  $h_{\text{vol}}(R_s)$  are of particular interest for the analysis and understanding the electrochemical system and are defined as follows [Eqs. (13) and (14)]:

$$h_{\text{vol}}(R_s) = \frac{f_{\text{num}}(R_s) \cdot R_s^3}{\int_0^\infty f_{\text{num}}(R_s) \cdot R_s^3 dR_s} \quad (13)$$

$$h_{\text{area}}(R_s) = \frac{f_{\text{num}}(R_s) \cdot R_s^2}{\int_0^\infty f_{\text{num}}(R_s) \cdot R_s^2 dR_s} \quad (14)$$

The mean values  $\bar{R}_s^{\text{num}}$ ,  $\bar{R}_s^{\text{area}}$ , and  $\bar{R}_s^{\text{vol}}$  of the fraction density functions are determined using [Eq. (15)]:

$$\bar{R}_s = \int_0^\infty R_s \cdot h(R_s) dR_s \quad (15)$$

To extend the presented single-particle model by the effect of diffusion in multiple particles, the diffusion Equation (1) is considered for every particle with the radius  $R_s$  as [Eq. (16)]:

$$\frac{\partial c_{\text{Li}_e^+}(r, R_s)}{\partial t} = \frac{1}{r^2} \frac{\partial}{\partial r} \left( D_s r^2 \frac{\partial c_{\text{Li}_e^+}(r, R_s)}{\partial r} \right) \quad (16)$$

The electrode potential at every particle of the size  $R_s$  is the same (compare the model assumptions in Table 1) so that reaction overpotential and reaction rate only depend on the local activities, which themselves are functions of the surface concentration at the particle surface. Concentration values are particularly affected by state of charge (SOC) and diffusion within a single particle. This results in the modified definition of boundary conditions for different particles as  $-D_s \frac{\partial c_{\text{Li}_e^+}}{\partial r}(r = R_s, R_s) = J^{\text{Li}}(R_s)/F$ . The reaction density  $j^{\text{Li}}$  is finally determined by [Eq. (17)]:

$$j^{\text{Li}} = \int_0^\infty f_{\text{area}}(R_s) J^{\text{Li}}(R_s) dR_s \quad (17)$$

### Degradation model

Degradation at the electrode level is modeled. This includes a change of the electrode structure (i.e., change of PSD) and a change of the active material fraction  $\varepsilon_s$  (i.e., electrical disconnection). These effects can be caused by particle cracking and agglomeration through degradation processes such as solvent co-intercalation or mechanical stress through volume changes during lithiation. The structural change is modeled by applying population balances, as provided by Marchisio et al. [Eq. (18)].<sup>[17]</sup>

$$\frac{\partial f_{\text{num}}(R_s)}{\partial t} = B^{\text{agl}}(R_s) - D^{\text{agl}}(R_s) + B^{\text{cr}}(R_s) - D^{\text{cr}}(R_s) \quad (18)$$

This population balance includes birth and death through aggregation and cracking as follows [Eqs. (19)–(22)]:

$$B^{\text{agl}}(R_s) = \frac{R_s^2}{2} \int_0^{R_s} \frac{\beta^{\text{agl}}((R_s^3 - P_s^3)^{\frac{1}{3}}, P_s)}{(R_s^3 - P_s^3)^{\frac{2}{3}}} \cdot f_{\text{num}}((R_s^3 - P_s^3)^{\frac{1}{3}}) f_{\text{num}}(P_s) dP_s \quad (19)$$

$$D^{\text{agl}}(R_s) = f_{\text{num}}(R_s) \int_0^\infty \beta^{\text{agl}}(P_s, R_s) f_{\text{num}}(P_s) dP_s \quad (20)$$

$$B^{\text{cr}}(R_s) = \int_{R_s}^\infty \alpha^{\text{cr}}(P_s) b^{\text{act}}(R_s|P_s) f_{\text{num}}(P_s) dP_s \quad (21)$$

$$D^{\text{cr}}(R_s) = \alpha^{\text{cr}}(R_s) f_{\text{num}}(R_s) \quad (22)$$

with the aggregation kernel  $\beta^{\text{agl}}$ , cracking kernel  $\alpha^{\text{cr}}$ , and number of active fragments  $b^{\text{act}}$  with the radius  $R_s$  through the cracking of a particle with the radius  $P_s$ . The resulting fragments can be either connected (i.e., active) or electrically disconnected fragments  $b^{\text{dis}}$ , which in the latter case results in a decrease of the active material fraction  $\varepsilon_s$  by [Eq. (23)]:

$$\frac{\partial \varepsilon_s}{\partial t} = - \int_0^\infty \left[ \int_{R_s}^\infty \alpha^{\text{cr}}(P_s) b^{\text{dis}}(R_s|P_s) f_{\text{num}}(P_s) dP_s \right] V_s(R_s) dR_s \quad (23)$$

The actual evolution of the PSD during battery usage can be very complex and depends on many system properties (e.g., the tendency of solvent to co-intercalate, surface properties, surface films, active material stiffness, etc.). As a result of this complexity, detailed experiments or simulations are needed to provide a quantitative analysis of electrode degradation. As this is out of the scope of this study, general scenarios and their impact on electrode performance are simulated.

### Simulations

As the aim of this study is to provide a fundamental and general view of the performance and degradation of graphite electrodes, the system parameters and simulations are described in detail.

### Parameters

Several material properties are needed for model parameterization. The diffusion coefficient of graphite materials commonly used in simulations ranges orders of magnitude from  $2 \times 10^{-16}$ – $5 \times 10^{-9} \text{ m}^2 \text{ s}^{-1}$ .<sup>[21,22,25–28]</sup> Experimental results for mesocarbon microbeads (MCMB) suggest diffusion coefficients of  $1 \times 10^{-15}$ – $1 \times 10^{-13} \text{ m}^2 \text{ s}^{-1}$ .<sup>[29]</sup> Good agreement with discharge curves by simulations is often obtained by rather small diffusion coefficients. Furthermore, the effect of the PSD is more distinct with a smaller diffusion coefficient. Therefore, a diffusion coefficient is chosen at the lower bound of the experimentally determined coefficients with  $1 \times 10^{-15} \text{ m}^2 \text{ s}^{-1}$ . Nevertheless, it needs to be emphasized that the presented effects of the PSD on the performance of graphite electrodes may be less distinct for graphite materials with faster solid diffusion.

Standard chemical potentials for Li, vacancies, and electrons are provided by Colclasure and Kee.<sup>[22]</sup> The standard concentration of Li and vacancies in graphite are defined as their maximum concentrations  $c_{\text{max}}$  and for Li in the electrolyte as  $1200 \text{ mol m}^{-3}$ . The nonideality of Li and vacancy activity in graphite is provided by the Redlich Kister coefficients.<sup>[22]</sup> The rate of the ideal concentration-dependent exchange current density is given in Ref. [22] with  $k_{\text{ct}} = 1.429 \times 10^{-9} \text{ m}^{2.5} \text{ mol}^{-0.5} \text{ s}^{-1}$  based on experimental data from Ref. [27]. The ideal exchange current density assumes an ideal activity  $a_i = c_i/C_i^0$  and can be written as [Eq. (24)]:

$$i_0^{\text{ideal}} = k_{\text{ct}} F (c_{\text{Li}_i^+})^{\beta_a} (c_{\text{max}} - c_{\text{Li}_i})^{\beta_a} (c_{\text{Li}_i})^{\beta_c} \quad (24)$$

Nonideal exchange current density, as applied in this work, includes the nonideality of activity through Equation (4) and can be written as [Eq. (25)]:

$$i_0 = c_{\text{max}} F k_a \exp\left(\frac{\Delta G^0 \beta_a}{RT}\right) a_{\text{Li}_i^+}^{\beta_a} a_{\text{V}_s}^{\beta_a} a_{\text{Li}_i}^{\beta_c} \quad (25)$$

If the assumption for ideal activity coefficients is applied to Equation (25) this leads to another representation of Equation (24) [Eq. (26)]:

$$i_0^{\text{ideal}} = c_{\text{max}} F k_a \exp\left(\frac{\Delta G^0 \beta_a}{RT}\right) \frac{(c_{\text{Li}_i^+})^{\beta_a}}{(C_{\text{Li}_i^+}^0)^{\beta_a}} \frac{(c_{\text{max}} - c_{\text{Li}_i})^{\beta_a}}{(C_{\text{V}_s}^0)^{\beta_a}} \frac{(c_{\text{Li}_i})^{\beta_c}}{(C_{\text{Li}_i}^0)^{\beta_c}} \quad (26)$$

and thus the given parameter for the reaction rate constant  $k_{\text{ct}}$  can be used to determine the rate constant  $k_a$  of the nonideal exchange current density [Eq. (27)]:

$$k_a = k_{ct} \frac{(C_{Li_s}^0)^{\beta_c} (C_{V_s}^0)^{\beta_a} (C_{Li_e}^0)^{\beta_a}}{c_{max}} \exp\left(\frac{-\Delta G^0 \beta_a}{RT}\right) \quad (27)$$

All parameters used are listed in Table 2.

| Table 2. Parameters for mathematical models.  |                                    |
|---|------------------------------------|
| Parameter   | Value                              |
| $T$ [K]   | 300 (chosen)                       |
| solid diffusion coefficient $D_s$ [ $m^2 s^{-1}$ ]                                    | $1 \times 10^{-15}$ (chosen)       |
| ideal exchange current density rate $k_{ct}$ [ $m^{2.5} mol^{-0.5} s^{-1}$ ]          | $1.429 \times 10^{-9}$ , Ref. [22] |
| anodic transfer coefficient $\beta^a$ [-]   | 0.5 (chosen)                       |
| cathodic transfer coefficient $\beta^c$ [-]   | 0.5 (chosen)                       |
| double layer capacitance $C^{DL}$ [ $F m^2$ ]   | 0.2, Ref. [21]                     |
| active material volume fraction $\varepsilon_s$ [-]                                   | 0.6 (chosen)                       |
| Standard chemical potential of Li in solid $\mu_{Li_s}^0$ [ $J mol^{-1}$ ]            | $-1.165 \times 10^4$ , Ref. [22]   |
| standard chemical potential of Li ions in electrolyte $\mu_{Li_e}^0$ [ $J mol^{-1}$ ] | 0, Ref. [22]                       |
| standard chemical potential of vacancy in solid $\mu_{V_s}^0$ [ $J mol^{-1}$ ]        | 0, Ref. [22]                       |
| standard chemical potential of electron $\mu_{e_s}$ [ $J mol^{-1}$ ]                  | 0, Ref. [22]                       |
| concentration Li ions in electrolyte $c_{Li_e}$ [ $mol m^{-3}$ ]                      | 1200, Ref. [21]                    |
| maximum concentration of Li and vacancies in solid $C_{max}$ [ $mol m^{-3}$ ]         | 16 100, Ref. [22]                  |
| start concentration of Li in solid $c_{Li_s}(0)$ [ $mol m^{-3}$ ]                     | 13 098 (chosen)                    |
| maximum theoretical discharge capacity $c_{ah}$ [Ah]                                  | $c_s(0) F \varepsilon_s$           |
| scale parameters $\lambda$ [ $\mu m$ ]  | 1.25, 2.5, 5, 10, 20 (chosen)      |
| shape parameters $k$ [-]  | 8, 4, 2, 1.5 (chosen)              |

The figure shows the correlation between  $\lambda$  and  $k$  and their influence on  $R_s^{50}$  and  $R_s^{90}$ . In this work, the performance of graphite electrodes is investigated for different theoretical Weibull distributions within the presented typical range of PSD.

### Degradation

The impact of a hypothetical change of the PSD through agglomeration and cracking is analyzed. This degradation analysis does not aim to provide actual quantitative data of electrode degradation, but rather to point out the fundamental differences between both processes. Both scenarios are applied with constant kernels for particle cracking  $\alpha^{cr} = 0.5$  in cracks simulation run time and agglomeration  $\beta^{agl} = 0.5$  in  $(n_s)^{-1}$  in agglomerations  $m^3$  per degradation simulation run time. Furthermore, in the case of particle cracking, a disconnection of one part of the particle can be expected.<sup>[3,9]</sup> For particle cracking, in this scenario the particle breaks into two particles of the same size, one of which is still connected electrically and the other one is disconnected. This is based on a symmetric fragmentation, as given by Marchisio et al.,<sup>[17]</sup> and leads to [Eqs. (29) and (30)]:

$$b^{act}(R_s|P_s) = b^{dis}(R_s|P_s) \quad (29)$$

$$b^{act}(R_s|P_s) = \begin{cases} 1 & \text{if } \frac{P_s}{2^k} = R_s \\ 0 & \text{if } \frac{P_s}{2^k} \neq R_s \end{cases} \quad (30)$$

### Particle size distribution

The effect of the PSD on the electrode structure is investigated within the usual range for graphite materials. To compare different PSDs, the theoretical capacity and thus the amount of active material needs to be fixed. Therefore, the active material fraction is chosen with  $\varepsilon_s = 0.6$  as a PSD-independent parameter.

A good indicator for the properties of a PSD is the  $R_{50}$  value and the  $R_{50}/R_{90}$  ratio. A plot of  $R_{50}$  versus  $R_{90}$  for different graphite materials reported previously<sup>[30,31]</sup> is shown in Figure 1 A. The arrow indicates a PSD of MCMB given by Baohua et al.,<sup>[30]</sup> which is shown in Figure 1 B and includes a fit by application of the Weibull distribution [Eq. (28)]:

$$h_{num}(R_s) = \frac{k}{\lambda} \cdot \left(\frac{R_s}{\lambda}\right)^{k-1} \cdot \exp\left[-\left(\frac{R_s}{\lambda}\right)^k\right] \quad (28)$$

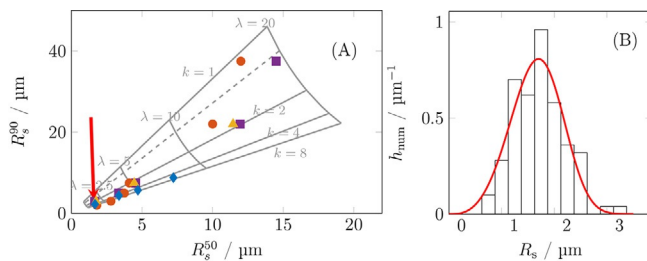


Figure 1. (A) Typical values for  $R_s^{50}$  and  $R_s^{90}$  for different graphites: E-LSG ( $\blacktriangle$ ),<sup>[31]</sup> SFG ( $\blacksquare$ ),<sup>[31]</sup> KS ( $\bullet$ ),<sup>[31]</sup> and MCMB ( $\blacklozenge$ )<sup>[30]</sup> that includes the corresponding values of Weibull distributions in this range. (B) PSD of a MCMB taken from Ref. [30] that includes a fit of a Weibull distribution (—).

The impact of the solid–electrolyte interface (SEI) can be neglected because it is mainly formed from the electrolyte and Li provided by the positive electrode. This denotes that the SEI instead impacts the amount of cyclable Li in the counter electrode than the actual storage capacity of the graphite electrode, which is investigated here.

### Numerical solution

For numerical solution, equations are discretized in finite volumes in the  $r$  domain. Furthermore, the continuous PSD is approximated by a finite number of particle size groups each of which have a certain homogeneous particle size, similar to that shown in Figure 1 B. The quantity of intermediate particles is approximated by linear interpolation. This interpolation is also used to treat products of particle cracking, which have a size in between two groups. Time derivatives are solved with an adaptive explicit ode solver with MATLAB.

## Results and Discussion

## Impact of the particle size distribution

The presented models enable us to study the electrode potential during the discharge process as shown in Figure 2 for a graphite electrode. The electrode potential of a graphite electrode versus a Li reference, as simulated here, increases during discharge. The maximum electrode capacity is defined

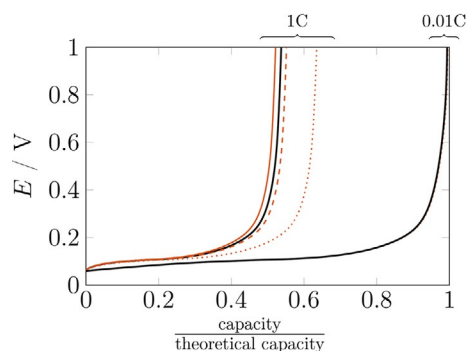


**Figure 2.** Electrode potential during discharge process for different C-rates applied shown for the accurate consideration of the PSD using a multiple-particle model (—) and its approximation using a single-particle model based on mean radii based on number (•••••), surface area (---), and volume (—).

at a cut-off voltage of 1 V. Higher electrode potentials are usually evoked by higher internal reaction or diffusion resistances and imply a worse electrode performance and a lower maximum discharge electrode capacity. The maximum theoretical discharge capacity  $C_{Ah}$  is used to define a dimensionless electrode capacity. Reaction and diffusion resistances decrease with decreasing charging rates, as can be seen in Figure 2, in which the dimensionless electrode capacity is almost 1 for C-rates of 0.01 C but is considerably lower for higher rates of 1 C.

The PSD scale of the Weibull distribution is defined by the parameter  $\lambda$ . Large  $\lambda$  values denote large-scale distributions, that is, a large distribution width and large mean radius. The impact of the distribution scale is shown in Figure 3. If the width of the PSD is increased, the electrode capacity decreases. Additionally, the potential of the plateau is higher with larger  $\lambda$  values, which can also be confirmed by experimental results.<sup>[31]</sup> Both effects are caused by higher internal resistances through longer diffusion pathways in larger particles and a smaller specific surface area  $a_s$  in distributions with larger particles. The impact of the PSD shape on the electrode capacity is shown in Figure 4. This shows that the change in the electrode capacity dependent on shape parameter  $k$  for different PSD scales  $\lambda$ . It can be seen, that capacity increases with increasing shape parameter  $k$ , that is, decreasing width of PSD, while maintaining almost constant number-based mean radius. In addition, the gradient in this case is larger for smaller  $k$  and  $\lambda$  values. The decrease in the maximum electrode capacity is caused by an increasing

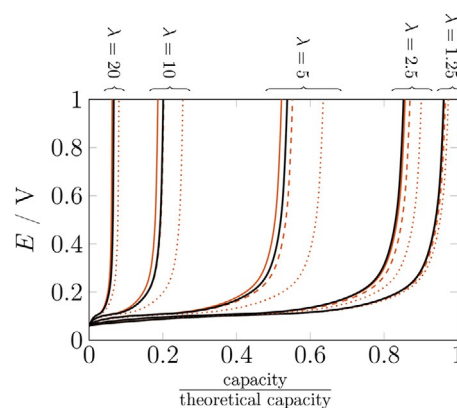


**Figure 3.** Electrode potential during the discharge process for differently scaled PSDs shown for accurate consideration of the PSD using a multiple-particle model (—) and its approximation using a single-particle model based on mean radii based on number (•••••), surface area (---), and volume (—).

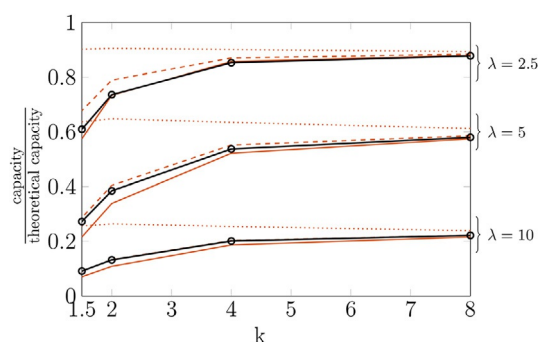


**Figure 4.** Electrode discharge capacity dependent on PSD shape shown for differently scaled PSDs with accurate consideration of the PSD using a multiple-particle model (—) and its approximation using a single-particle model based on mean radii based on number (•••••), surface area (---), and volume (—).

number of larger particles that have longer diffusion pathways and leads to a lower specific surface area of the PSD. Electrode capacities for all PSDs investigated with a C-rate of 1 C are provided in Table 3. The best electrode performance is obtained for PSDs with large  $k$  and small  $\lambda$  values, that is, narrow distributions with small mean particle radii. This denotes that it may be beneficial to tune the electrode particle size by reducing the amount of large particles.

As an accurate consideration of the PSD, the use of a multiple-particle model is much more expensive computationally than the use of a single-particle model, and often an approximation using a single-particle model is preferable. Different approaches to determine a mean radius are possible and are, in general, based on number, surface area, or volume distributions. To evaluate how far they can represent the multiple-particle behavior accurately, we compare the simulation results introduced previously obtained by using the multiple-particle model with results generated by using a single-particle model with different approximations of the mean particle

**Table 3.** Electrode discharge capacity for 1 C discharge with different shape and scale parameters of the PSD for the multiple-particle model and the single-particle model with different approximations for the particle radius based on number, surface area and volume.

| Shape     | Model approach                    | $\lambda = 1.25$ | $\lambda = 2.5$ | $\lambda = 5$ | $\lambda = 10$ | $\lambda = 20$ |
|-----------|-----------------------------------|------------------|-----------------|---------------|----------------|----------------|
| $k = 8$   | PSD                               | 0.968            | 0.878           | 0.58          | 0.222          | 0.072          |
|           | $R_s^{\text{num}}$ approximation  | 0.972            | 0.893           | 0.612         | 0.239          | 0.077          |
|           | $R_s^{\text{area}}$ approximation | 0.97             | 0.884           | 0.586         | 0.222          | 0.072          |
| $k = 4$   | $R_s^{\text{vol}}$ approximation  | 0.969            | 0.879           | 0.575         | 0.216          | 0.07           |
|           | PSD                               | 0.961            | 0.853           | 0.537         | 0.201          | 0.067          |
|           | $R_s^{\text{num}}$ approximation  | 0.974            | 0.901           | 0.635         | 0.254          | 0.081          |
| $k = 2$   | $R_s^{\text{area}}$ approximation | 0.966            | 0.87            | 0.552         | 0.203          | 0.067          |
|           | $R_s^{\text{vol}}$ approximation  | 0.963            | 0.857           | 0.522         | 0.187          | 0.063          |
|           | PSD                               | 0.924            | 0.736           | 0.385         | 0.132          | 0.052          |
| $k = 1.5$ | $R_s^{\text{num}}$ approximation  | 0.975            | 0.905           | 0.648         | 0.264          | 0.084          |
|           | $R_s^{\text{area}}$ approximation | 0.946            | 0.789           | 0.404         | 0.133          | 0.051          |
|           | $R_s^{\text{vol}}$ approximation  | 0.931            | 0.734           | 0.338         | 0.108          | 0.046          |
| $k = 1.5$ | PSD                               | 0.868            | 0.61            | 0.272         | 0.091          | 0.044          |
|           | $R_s^{\text{num}}$ approximation  | 0.974            | 0.902           | 0.637         | 0.256          | 0.081          |
|           | $R_s^{\text{area}}$ approximation | 0.914            | 0.678           | 0.287         | 0.091          | 0.043          |
|           | $R_s^{\text{vol}}$ approximation  | 0.88             | 0.575           | 0.216         | 0.07           | 0.04           |

radius, that is,  $\bar{R}_s^{\text{num}}$ ,  $\bar{R}_s^{\text{area}}$ , and  $\bar{R}_s^{\text{vol}}$ . The curves for low C-rates all overlap (Figure 2). As a result of very low kinetic losses, there is no considerable deviation between both models and different approximations. In contrast, at higher C-rates, the simulation results differ considerably. The surface-area- and volume-based mean approximations slightly overestimate and underestimate the electrode potential, respectively. In contrast, the electrode potential is clearly underestimated by the number-based mean approximation, which leads to a significantly overestimated maximum capacity. The results indicate that the observed deviations are less distinct with small and large PSDs than for intermediate values of  $\lambda$  (Figure 3). Furthermore, particularly for the results shown in Figure 3, it can be seen that for small-scale PSDs volume-based approximations reproduce electrode capacity accurately, whereas for large-scale PSDs, surface-area-based approximations agree almost perfectly with the results of the multiple-particle model. The volume-based mean approximation uses the most representative particle size in terms of particle volume and, therefore, provides a good approximation for the diffusion pathway and diffusion-induced internal resistance. The reason for the good agreement of surface-area-based mean  $\bar{R}_s^{\text{area}}$  is because of its direct correlation to specific surface area  $a_s$  [Eq. (31)]:

$$a_s = \int_0^\infty f_{\text{area}}(R_s) dR_s = \frac{3\varepsilon_s}{\bar{R}_s^{\text{area}}} \quad (31)$$

In the case of the dominating kinetic loss of reaction at the surface, this is a physically meaningful approximation. Thus the results as such indicate that internal resistance for a large-scale distribution is dominated by the high resistance of the surface reactions through low specific surface area. In contrast, diffusion limitations dominate for small-scale PSDs.

Furthermore, both approximations are useful to predict qualitatively the impact of the PSD shape in contrast to

a number-based mean approximation (Figure 4). The number-based mean approximation only for very large  $k$  values, that is, narrow PSDs, predicts electrode capacity accurately.

An overview of electrode capacities simulated with accurate consideration of the PSD using the multiple-particle model and the approximations using the single-particle model is given in Table 3. The provided data shows that number-based mean approximations are only accurate for a few cases of narrow distributions. Surface-area-based approximations have small deviations for large-scale distributions, and volume-based approximations have small deviations for small-scale distributions. Single-particle approximations are the least accurate for intermediate-scale and coarse distributions. The presented results suggest that in the case of a surface reaction or solid diffusion-limited electrodes, surface-area- or volume-based mean approximations should be used, respectively.

### Local current density

As a result of the change of the surface-area-to-volume ratio for different sized particles, heterogeneity in local surface current density can be expected. Goers et al.<sup>[9]</sup> investigated the existence of such a surface current density distribution and studied its effect on the exfoliation behavior of graphite electrodes. Exfoliation is caused by solvent co-intercalation as the intercalation reactions depends on local overpotentials caused by deviations in surface activity, concentration of Li, and vacancies, which is affected mainly by diffusion kinetics inside a particular particle. This leads to heterogeneous passivation, that is, SEI layer growth.<sup>[9,32]</sup> The reason for some particles to passivate or exfoliate may be explained by deviations in current density.<sup>[9]</sup> To evaluate local current densities on particle surfaces for different PSDs, the surface area fraction density  $h_{\text{area}}$  and surface current densities  $J^{\text{Li}}(R_s)$  for a 1 C discharge process are shown in Figure 5. The surface area fraction density is shown together with surface current density because it indicates the actual fraction of a local current density on the total surface area. The current density is shown at the end of discharge for distributions with the shape parameters  $k = 8, 4, 2,$  and  $1.5$  (Figure 5 A–D, respectively). Furthermore, the impact of differently scaled PSDs, that is, scale parameter  $\lambda = 1.25$  and  $20$ , are presented. In general, with larger-scaled PSDs, that is, larger  $\lambda$  values, current densities are larger, and with coarser PSDs, that is, smaller  $k$  values, current densities differ more significantly between differently sized particles. If we focus on the narrow distributions shown in Figure 5 A and B, it can be seen that in large-scale PSDs current density is almost constant within the PSD range, whereas for smaller-scale PSDs the current can be considerably larger for larger particles than for smaller ones. This indicates a higher impact of diffusion processes in the particle volume at smaller-scale PSDs and is supported by the good approximation through volume-based means for

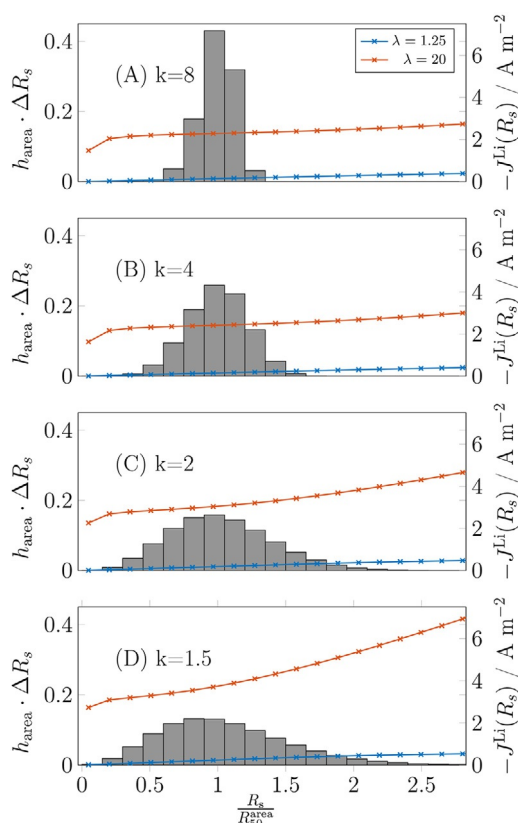


**Figure 5.** Local surface current density and surface area fraction density shown for different particle shapes and differently scaled PSDs at the end of discharge, where (A), (B), (C), and (D) show results for alternating shape parameters  $k=8$ ,  $k=4$ ,  $k=2$ , and  $k=1.5$ , respectively.

such distributions reported previously. Even larger differences in local current density can be observed in coarser PSDs in Figure 5C and D, which is supported by the experiments of Buqa et al.<sup>[31]</sup>, which show a high extent of exfoliation for a coarse PSD. The presented simulation results indicate the highest current densities in coarse and large-scale PSDs at the larger particles, which can also explain why a significantly lower degree of exfoliation is found at the smaller particles in experiments.<sup>[9]</sup>

We focus on the coarse distribution in Figure 6 as the observed effects are most distinct there. The change of surface current densities during the discharge process is shown for large- and small-scale PSDs. The results indicate that in large-scale distributions, current density is highest at the beginning of discharge and then adjusts between small and large particles, whereas it is the opposite and less distinct for small-scale distributions. This denotes that, in particular for large-scale PSDs, the actual charging/discharging can be critical in terms of high local surface current densities. Furthermore, it can be seen that at the end of discharge, the current density decreases beginning with the smallest particles and increases at the largest particles as long as the cut-off voltage is not reached. To sum up, the presented analysis of current density with different PSDs shows a good agreement with experimental studies<sup>[9,31]</sup> that to avoid high current density and thus degradation processes such as exfoliation, small-scale

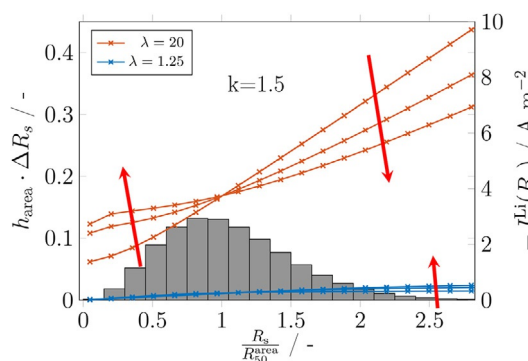


**Figure 6.** Local surface current density and surface area fraction density shown for particle shape  $k=1.5$  and differently scaled PSDs with  $\lambda=1.25$  and 20. Current densities are shown as it changes during the discharge process for one third discharge, two thirds discharge, and full discharge, and the direction of change is indicated by red arrows.

and narrow PSDs should be favored, whereas high current densities at the beginning of discharge should be avoided.

### Degradation of electrode structure

The previous results show that PSDs should have a considerable impact on electrode performance and degradation processes such as solvent co-intercalation. This can cause graphite exfoliation or particle cracking.<sup>[3,9]</sup> A restructuring of the electrode morphology, that is, a change of the PSD, can impact electrode performance and result in decreased battery capacity during use. The resulting change of the PSD through the introduced cracking and agglomeration scenarios is shown in Figure 7, in which the original PSD refers to a reference PSD. If particle cracking occurs, the number of large

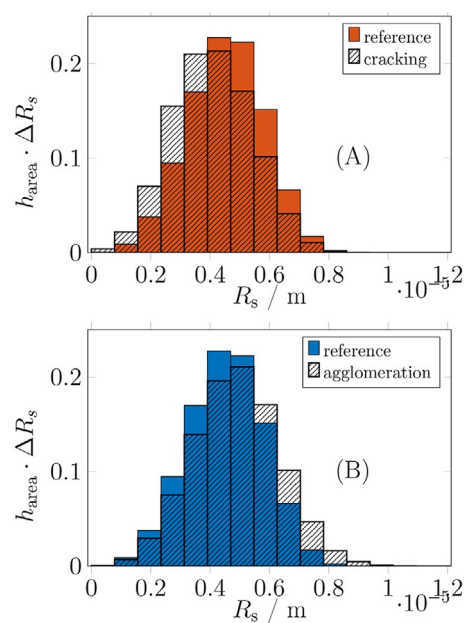


**Figure 7.** Number fraction density for a reference PSD and PSD after the change scenarios for (A) particle cracking and (B) agglomeration.

particles decreases as the number of smaller particles increases. Theoretically, and also observed experimentally, this process could go on until the electrode particles are broken into dust.<sup>[3]</sup> In general, this leads to a PSD with a higher surface-area-to-volume ratio and to loss of active material through electrical disconnection. Furthermore, a loss of cyclable Li in the disconnected particles would cause the unbalancing of the battery system. The effect of an unbalanced system is not considered in the single-electrode analysis presented here. Particle agglomeration causes a decrease of the number of smaller particles and an increase of larger particles but does not affect the active material fraction. As the active material content is constant, a change in electrode capacity is only caused by a change of internal resistances, such as diffusion or surface reactions.

The electrode capacity before and after both degradation scenarios is shown for different initial particle shapes and a constant particle scale of  $\lambda = 5$  in Table 4. The electrode capacity is further presented to be dependent on C-rate to show the impact on electrode kinetics. It can be seen that for very low C-rates, only in the case of particle cracking does the electrode capacity decrease because the active material fraction for agglomeration stays constant and internal resistances are very low at low rates. In contrast, for higher rates both scenarios impact electrode capacity considerably. Discharge capacities after degradation are comparably decreased for high rates, even so only for the case of particle cracking is active material lost. The effect of disconnected active material in the scenario of particle cracking is compensated partly through better electrode performance with smaller particles because of shorter diffusion pathways and a higher surface-area-to-volume ratio.

Our results demonstrate that a change of the PSD can be modeled using population balances. A realistic cracking and agglomeration needs to be set up and parameterized carefully to produce quantitative precise degradation scenarios. Nevertheless, in general, both degradation scenarios can lead to a decrease of electrode capacity for completely different reasons, which can be quantified by the charge-rate-dependent capacity.

**Table 4.** Electrode discharge capacity with different C-rates for reference scenarios with different initial PSD shape and degradation scenarios for cracking and agglomeration.

| Shape     | Scenario      | 0.01 C | 0.1 C | 1 C   |
|-----------|---------------|--------|-------|-------|
| $k = 8$   | reference     | 0.995  | 0.951 | 0.58  |
|           | agglomeration | 0.993  | 0.937 | 0.518 |
|           | cracking      | 0.774  | 0.734 | 0.419 |
| $k = 4$   | reference     | 0.994  | 0.94  | 0.537 |
|           | agglomeration | 0.992  | 0.927 | 0.484 |
|           | cracking      | 0.773  | 0.724 | 0.387 |
| $k = 2$   | reference     | 0.988  | 0.882 | 0.385 |
|           | agglomeration | 0.986  | 0.869 | 0.35  |
|           | cracking      | 0.768  | 0.673 | 0.274 |
| $k = 1.5$ | reference     | 0.978  | 0.802 | 0.272 |
|           | agglomeration | 0.975  | 0.787 | 0.25  |
|           | cracking      | 0.759  | 0.604 | 0.192 |

## Conclusions

In this work, we have introduced the particle size as a distributed parameter into a single particle electrode model for graphite electrodes to study the effect of the particle size distribution (PSD) on performance. The presented results show the impact of the shape and scale of the PSD on electrode performance. In general, small-scale PSDs show lower internal resistances and smaller local surface current densities. This implies that they provide a higher electrode capacity and lower probability for degradation processes related to local current densities such as solvent co-intercalation. It was further shown that in smaller-scale PSDs, diffusion processes determine the electrode resistance, whereas in larger-scale PSDs, surface reactions are limiting through small specific surface areas. In general, the results indicate that for a graphite electrode, the surface-area- or volume-based mean approximations used commonly with the single-particle approach are accurate over a wide range of PSDs and differ considerably only for coarse distributions from accurate considerations with multiple-particle approaches. Therefore, we conclude, that as long as the PSD is not exceedingly coarse, the surface-area- and volume-based approximations predict electrode capacity sufficiently accurately for large- and small-scale PSDs. Analysis of the theoretical local current densities indicates that the highest current densities occur at large particles in coarse and large-scale distributions at the beginning of discharge.

As large current densities can lead to degradation through the restructuring of the electrode morphology, we provide an approach based on population balance to investigate the effect of a transient change of the PSD. Example scenario-based simulations show that both particle agglomeration and particle cracking can lead to a decrease of electrode capacity, although the fundamental reasons for the loss of active material and increase of internal resistance can be very different. Based on these results, we suggest that the effect of the PSD should be considered if degradation processes are analyzed in Li-ion batteries and its effect on performance. Both the uneven degradation at differently sized particles because of the diversity of the surface current density and the change of the distribution during battery operation are, therefore, of particular interest.

## List of Symbols

### Latin letters

|  |   |
|--|---|
| $a_s$ [ $\text{m}^{-1}$ ]                          | specific surface area                   |
| $a_i$ [-]  | activity of species $i$                 |
| $A_s$ [ $\text{m}^2$ ]                             | solid particle surface area             |
| $b^{\text{act}}$ [ $\text{m}^{-1}$ ]               | active fragments through cracking       |
| $b^{\text{dis}}$ [ $\text{m}^{-1}$ ]               | disconnected fragments through cracking |
| $B^{\text{agl}}$ [ $\text{s}^{-1} \text{m}^{-4}$ ] | birth rate through agglomeration        |
| $B^{\text{cr}}$ [ $\text{s}^{-1} \text{m}^{-4}$ ]  | birth rate through cracking             |
| $c_s$ [ $\text{mol m}^{-3}$ ]                      | Li concentration in solid,              |
| $c_{\text{max}}$ [ $\text{mol m}^{-3}$ ]           | maximum concentration in solid          |

|  |   |
|--|---|
| $C_{DL}$ [F m <sup>-2</sup> ]                                    | double layer capacitance  |
| $C_i^0$ [mol m <sup>-3</sup> ]                                   | standard state concentration of species $i$                         |
| $D^{agl}$ [s <sup>-1</sup> m <sup>-4</sup> ]                     | death rate through agglomeration                                    |
| $D^{cr}$ [s <sup>-1</sup> m <sup>-4</sup> ]                      | death rate through cracking   |
| $E$ [V]  | electrode potential   |
| $f_{num}$ [m <sup>-4</sup> ]                                     | number density  |
| $f_{area}$ [m <sup>-2</sup> ]                                    | surface area density  |
| $f_{vol}$ [m <sup>-1</sup> ]                                     | volume density  |
| $F$ [C mol <sup>-1</sup> ]                                       | Faraday constant  |
| $h$ [m <sup>-1</sup> ]   | fraction density  |
| $h_{num}$ [m <sup>-1</sup> ]                                     | number fraction density   |
| $h_{area}$ [m <sup>-1</sup> ]                                    | surface area fraction density                                       |
| $h_{vol}$ [m <sup>-1</sup> ]                                     | volume fraction density   |
| $D_s$ [m <sup>2</sup> s <sup>-1</sup> ]                          | solid diffusion coefficient   |
| $i_0$ [A m <sup>-2</sup> ]                                       | exchange current density  |
| $i_0^{ideal}$ [A m <sup>-2</sup> ]                               | ideal exchange current density                                      |
| $\hat{I}$ [A m <sup>-3</sup> ]                                   | applied current density   |
| $j^{Li}$ [A m <sup>-3</sup> ]                                    | Li current density  |
| $J^{Li}$ [A m <sup>-2</sup> ]                                    | Li surface current density  |
| $k$ [-]  | shape parameter   |
| $k_{ct}$ [m <sup>2.5</sup> mol <sup>-0.5</sup> s <sup>-1</sup> ] | ideal exchange current density rate constant                        |
| $k_a$ [m s <sup>-1</sup> ]                                       | anodic reaction rate constant                                       |
| $k_c$ [m <sup>4</sup> mol <sup>-1</sup> s <sup>-1</sup> ]        | cathodic reaction rate constant                                     |
| $ns$ [m <sup>-3</sup> ]  | total particle density  |
| $r$ [m]  | radial coordinate   |
| $R_s$ [m]  | solid particle radius   |
| $R_{50}$ [m]   | particle radius at which 50% of the number of particles are smaller |
| $R_{90}$ [m]   | particle radius at which 90% of the number of particles are smaller |
| $\bar{R}_s^{num}$ [m]  | number-based mean   |
| $\bar{R}_s^{area}$ [m]   | surface-area-based mean   |
| $\bar{R}_s^{vol}$ [m]  | volume-based mean   |
| $R$ [J mol <sup>-1</sup> K <sup>-1</sup> ]                       | ideal gas constant  |
| $P_s$ [m]  | second radius   |
| $V_s$ [m <sup>3</sup> ]  | solid particle volume   |

### Greek letters

|   |  |
|---|--|
| $\alpha^{cr}$ [(runtime) <sup>-1</sup> ]                | cracking kernel                                  |
| $\beta_a$ [-]   | anodic transfer coefficient                      |
| $\beta_c$ [-]   | cathodic transfer coefficient                    |
| $\beta^{agl}$ [m <sup>3</sup> (runtime) <sup>-1</sup> ] | agglomeration kernel                             |
| $\varepsilon_s$ [-]                                     | solid volume fraction                            |
| $\Delta G^0$ [J mol <sup>-1</sup> ]                     | change in Gibbs free energy                      |
| $\Delta R_s$ [m]  | radius difference of discretization              |
| $\lambda$ [μm]  | scale parameter                                  |
| $\mu_i^0$ [J mol <sup>-1</sup> ]                        | standard state chemical potential of species $i$ |

### Acknowledgements

We would like to thank the Nds. Ministerium für Wissenschaft und Kultur of the State of Lower Saxony for the financial support of this work with Graduiertenkolleg Energiespeicher und Elektromobilität Niedersachsen (GEENI).

**Keywords:** batteries • electrochemistry • electrodes • graphite • particle size distribution <

- [1] G. T.-K. Fey, Y. G. Chen, H.-M. Kao, *J. Power Sources* **2009**, *189*, 169–178.
- [2] T. Drezen, N.-H. Kwon, P. Bowen, I. Teerlinck, M. Isono, I. Exnar, *J. Power Sources* **2007**, *174*, 949–953.
- [3] D. Aurbach, B. Markovsky, I. Weissman, E. Levi, Y. Ein-Eli, *Electrochim. Acta* **1999**, *45*, 67–86.
- [4] J. Vetter, P. Novák, M. R. Wagner, C. Veit, K. C. Möller, J. O. Besenhard, M. Winter, M. Wohlfahrt-Mehrens, C. Vogler, A. Hammouche, *J. Power Sources* **2005**, *147*, 269–281.
- [5] B. Michalak, H. Sommer, D. Mannes, A. Kaestner, T. Brezesinski, J. Janek, *Sci. Rep.* **2015**, *5*, 15627.
- [6] W.-R. Liu, Z.-Z. Guo, W.-S. Young, D.-T. Shieh, H.-C. Wu, M.-H. Yang, N.-L. Wu, *J. Power Sources* **2005**, *140*, 139–144.
- [7] Z. Wu, W. Ren, L. Wen, L. Gao, J. Zhao, Z. Chen, G. Zhou, F. Li, H.-M. Cheng, *ACS Nano* **2010**, *4*, 3187–3194.
- [8] H. Li, X. Huang, L. Chen, G. Zhou, Z. Zhang, D. Yu, Y. J. Mo, N. Pei, *Solid State Ionics* **2000**, *135*, 181–191.
- [9] D. Goers, M. E. Spahr, A. Leone, W. Märkle, P. Novák, *Electrochim. Acta* **2011**, *56*, 3799–3808.
- [10] V. Srinivasan, J. Newman, *J. Electrochem. Soc.* **2004**, *151*, A1517–A1529.
- [11] R. Darling, J. Newman, *J. Electrochem. Soc.* **1997**, *144*, 4201–4208.
- [12] M. Farkhondeh, C. Delacourt, *J. Electrochem. Soc.* **2012**, *159*, A177–A192.
- [13] M. Farkhondeh, M. Safari, M. Pritzker, M. Fowler, T. Han, J. Wang, C. Delacourt, *J. Electrochem. Soc.* **2014**, *161*, A201–A212.
- [14] M. Doyle, T. F. Fuller, J. Newman, *J. Electrochem. Soc.* **1993**, *140*, 1526.
- [15] T. G. Zavalis, M. Klett, M. H. Kjell, M. Behm, R. W. Lindström, G. Lindbergh, *Electrochim. Acta* **2013**, *110*, 335–348.
- [16] S. G. Rinaldo, P. Urchaga, J. Hu, W. Lee, J. Stumper, C. Rice, M. Eikerling, *Phys. Chem. Chem. Phys.* **2014**, *16*, 26876–26886.
- [17] D. L. Marchisio, R. D. Vigil, R. O. Fox, *J. Colloid Interface Sci.* **2003**, *258*, 322–334.
- [18] U. Krewer, D. Schröder, C. Weinzierl, *Comput. Aided Chem. Eng.* **2014**, *33*, 1237–1242.
- [19] M. Guo, G. Sikha, R. E. White, *J. Electrochem. Soc.* **2011**, *158*, A122–A132.
- [20] I. J. Ong, J. Newman, *J. Electrochem. Soc.* **1999**, *146*, 4360–4365.
- [21] N. Legrand, S. Raël, B. Knosp, M. Hinaje, P. Desprez, F. Lapique, *J. Power Sources* **2014**, *251*, 370–378.
- [22] A. M. Colclasure, R. J. Kee, *Electrochim. Acta* **2010**, *55*, 8960–8973.
- [23] M. M. Majdabadi, S. Farhad, M. Farkhondeh, R. A. Fraser, M. Fowler, *J. Power Sources* **2015**, *275*, 633–643.
- [24] D. Ramkrishna, *Population Balances: Theory and Applications to Particulate Systems in Engineering*, Academic Press, San Diego, **2000**.
- [25] K. Smith, C.-Y. Wang, *J. Power Sources* **2006**, *160*, 662–673.
- [26] Y. Xie, J. Li, C. Yuan, *J. Power Sources* **2014**, *248*, 172–179.
- [27] K. Smith, C.-Y. Wang, *J. Power Sources* **2006**, *161*, 628–639.
- [28] J. Christensen, J. Newman, *J. Electrochem. Soc.* **2004**, *151*, A1977–A1988.
- [29] M. Nishizawa, R. Hashitani, T. Itoh, T. Matsue, I. Uchida, *Electrochim. Solid-State Lett.* **1999**, *1*, 10–12.
- [30] B. Li, R. Guo, K. Li, C. Lu, L. Ling, *Prepr. Symp. - Am. Chem. Soc., Div. Fuel Chem.* **2002**, *47*, 187–188.
- [31] H. Buqa, A. Würsig, D. Goers, L. J. Hardwick, M. Holzappel, P. Novák, F. Krumeich, M. E. Spahr, *J. Power Sources* **2005**, *146*, 134–141.
- [32] M. E. Spahr, D. Goers, W. Märkle, J. Dentzer, A. Würsig, H. Buqa, C. Vix-Guterl, P. Novák, *Electrochim. Acta* **2010**, *55*, 8928–8937.

Received: April 1, 2016

Published online on September 8, 2016